Chapter 6

Other objects in the fields

With the GMRT field of view of $\sim 1^\circ.4$ at 327 MHz, maps of all the fields presented in this dissertation reveal a number of other compact as well extended objects. These objects include known HII regions, SNRs, background extragalactic objects and others which are not yet classified in any of these categories.

A list of compact sources from each of the fields along with their measured positions and 327-MHz flux densities is presented in this chapter. Where possible, flux densities at other frequencies have been used to determine the nature of these sources. The nature of other, unclassified source of extended emission seen in a few fields is then discussed, and suggestions for follow-up observations are made especially for Ultra compact HII (UC H II) regions.

6.1 Introduction

The Galactic longitude of all the observations presented in this dissertation were within $\pm 5^\circ$. The Galactic latitude of three out of the six independent pointings was within $\pm 0^\circ.2$, while the rest were at $> \pm 1^\circ$. Most of the emission from the Galactic plane at radio comes from many sources - (1) normal HII regions (Wink et al. 1982; Lockman 1989), (2) bright Ultra compact H II (UC H II) regions with a lower surface brightness extended emission (Wood & Churchwell 1989b; Kurtz et al. 1994), (3) compact HII regions with no detectable extended emission (Wink et al. 1983; Kuchar & Clark 1997), (4) SNRs (Green 2000), (5) background sources seen through the Galactic disk, and (6) the large scale Galactic background emission (Haslam et al. 1982). The $\sim 1^\circ.4$ field of view of GMRT observations at 327 MHz therefore reveal a number of compact as well as a few extended sources of emission.

The physical mechanism for the radio emission from HII regions and SNRs is, however, quite different. Radio emission from HII regions is due to the interaction between electrons and ions. The resulting thermal spectrum is almost flat (with a spectral index of ~ 0.1) at frequencies typically greater than ~ 1 GHz and turns over below this frequency due to free-free absorption by the intervening material. High resolution imaging of many compact HII regions reveal a halo surrounding a compact core (Wood & Churchwell 1989b). Detailed models of HII regions which include such temperature gradients and departure from LTE have been developed (Wilson & Jaeger 1987). However, these models have been applied only to objects where resolved images at a number of frequencies are available. High resolution multi frequency observations of HII regions, particularly of a larger sample of compact HII regions, will test these models more rigorously and provide improved estimates of the physical parameters. Most HII regions are also sources of radio recombination line (RRL) emission which has been detected at high radio frequencies (Caswell & Haynes 1987; Lockman 1989). Detection of high frequency RRL emission is one of the signatures used to identify H II regions. Emission from SNRs on the other hand is synchrotron radiation from free electrons accelerated to relativistic energies in the supernova shock front or due to the transfer of rotation energy from the neutron star, to the surrounding medium. The magnetic field in which the electrons move is also amplified. The spectral index is typically negative with no associated thermal or RRL emission.

The measured flux densities of all sources detected at 327 MHz, along with the 1420-MHz flux densities from NVSS images, are listed here. Two objects, namely G004.4+0.1 and G003.7−0.1, both catalogued as HII regions, reveal the core-halo morphology in the GMRT image and these GMRT observations constitute the first resolved low frequency images of these, possibly compact or UC H II regions.

6.2 Point sources in the fields

Tables 6.1 to 6.5 presents a list of point source flux densities at 327 MHz from the GMRT observations and 1420-MHz flux densities from the NVSS images. Reliable flux densities for point sources in the field of G001.4+0.0 were not available at either of these frequencies because of higher noise and poor image quality due to proximity to the Galactic centre. Also, no compact sources was detected in the field of G004.2−0.0. Data from IRAS and other RRL surveys have been used by Becker et al. (1994) to classify the compact

Table 6.1: List of point sources and their 327- and 1400-MHz flux densities in the field of G003.7−0.1

Name	RA$_{J2000}$ (h m s)	Dec$_{J2000}$ ($^\circ$ $'$ $''$)	S_{327} (mJy)	S_{1400} (mJy)
1756-2549	17 56 41.4	-25 49 10.9	99.5 ± 10	26.9 ± 1
1756-2542	17 56 38.1	-25 42 15.0	221.8 ± 10	70.7 ± 1
1755-2540	17 55 39.2	-25 40 44.0	207.9 ± 10	50.0 ± 1
1755-2535	17 55 22.3	-25 35 44.0	232.1 ± 10	6.0 ± 1
1755-2537	17 55 08.4	-25 37 24.0	108.1 ± 10	148.4 ± 1
1754-2539	17 54 56.3	-25 39 31.8	< 10	17.2 ± 1
1755-2543	17 55 10.2	-25 43 59.9	< 10	79.6 ± 1
1754-2534	17 54 39.4	-25 34 43.4	192.2 ± 10	31.2 ± 1
1754-2536	17 54 27.6	-25 36 23.2	177.7 ± 10	13.2 ± 1
1754-2540	17 54 10.7	-25 40 22.7	< 10	44.3 ± 1
1754-2544	17 54 10.4	-25 44 06.6	< 10	44.3 ± 1
1754-2556	17 54 46.4	-25 56 03.6	< 10	21.9 ± 1
1755-2557	17 55 19.9	-25 57 20.0	114.7 ± 20	16.1 ± 1
1755-2556	17 55 19.0	-25 56 56.0	78.1 ± 20	21.7 ± 1
1755-2551	17 55 09.6	-25 51 27.9	100.5 ± 30	11.4 ± 1
1755-2549	17 55 40.4	-25 49 52.0	< 10	11.6 ± 1
1754-2609	17 54 38.9	-26 13 47.5	183.3 ± 10	47.0 ± 1
1754-2609	17 54 36.4	-26 13 26.5	44.8 ± 10	47.0 ± 1

Table 6.2: List of point sources and their 327- and 1400-MHz flux densities in the field of G004.8+6.2

Name	RA$_{J2000}$ (h m s)	Dec$_{J2000}$ ($^\circ$ $'$ $''$)	S_{327} (mJy)	S_{1400} (mJy)
1732-21	17 32 53.7	-21 24 43.3	416 ± 60	22.7 ± 0.7
1732-22	17 32 19.4	-22 06 43.8	530 ± 50	274.0 ± 0.7
1734-21	17 34 04.0	-21 46 25.8	1120 ± 65	100.2 ± 1
1733-21	17 33 56.2	-21 42 41.3	716 ± 70	66.5 ± 0.7

Table 6.3: List of point sources and their 327- and 1400-MHz flux densities in the field of G356.2+4.5

Name	RA_{J2000} ($h\ m\ s$)	Dec_{J2000} ($^{\circ}\ '\ ''$)	S_{327} (mJy)	S_{1400} (mJy)
1715-29	17 15 04.7	-29 12 21.1	194.0 ± 20	297.1 ± 2
1716-29	17 16 11.6	-29 20 01.6	274.8 ± 20	242.5 ± 2
1715-29	17 15 14.3	-29 43 17.1	213.8 ± 20	157.1 ± 2
1715-29	17 16 52.5	-29 48 59.4	373.9 ± 20	124.5 ± 2
1757-30	17 17 57.6	-30 00 43.17	1053.9 ± 20	315.6 ± 2
1757-30	17 18 12.6	-30 01 43.97	812.5 ± 20	183.1 ± 2
1719-29	17 19 46.4	-29 52 49.1	91.6 ± 20	17.7 ± 2
1721-29	17 21 43.5	-29 35 16.9	294.0 ± 20	127.9 ± 2

sources as HII regions, UC H II regions and Planetary Nebula. These surveys, however, are confined to $|b| < 0^{\circ}.4$ and only two fields used in this dissertation, namely G003.7−0.2 and G001.4−0.1, overlap with these surveys. For these fields, additional data at 5 GHz from the Galactic plane surveys by Helfand et al. (1992); Becker et al. (1994) was also used.

The barrel-type SNR G003.7−0.2 (field of Table 6.1) was mapped by Gaensler (1999) at L-band using the VLA (`CnB` and `DnC` configurations with the smallest spacing of $\sim 0.12k\lambda$). This image was available from Astronomy Digital Image Library (ADIL)[1]. After correcting for the primary beam attenuation, it was used to obtain the 1420-MHz flux densities of compact sources in this field. The flux densities of compact sources measured from this image are listed in Table 6.1.

Most of the compact sources detected at 327 MHz show a negative spectral index, indicative of non-thermal nature of emission from these sources. A few compact sources detected at 1420 MHz are not detected at 327 MHz to a limit of $10 - 30$ mJy (the RMS noise in the images). These could be Galactic thermal sources or extragalactic sources with absorption due to the intervening Galactic ISM. Most of these sources are also weak and even if they have a flat spectrum till 327 MHz, they are below the detection limit of the 327 MHz observations.

[1] `http://adil.ncsa.uiuc.edu/`

Table 6.4: List of point sources and their 327- and 1400-MHz flux densities in the field of G356.2−1.5

Name	RA_{J2000} ($h\ m\ s$)	Dec_{J2000} ($^\circ\ '\ ''$)	S_{327} (mJy)	S_{1400} (mJy)
1740-3228	17 40 53.6	-32 28 13.9	177.9 ± 15	26.4 ± 5
1740-3334	17 40 56.3	-33 34 44.8	131.6 ± 15	51.3 ± 2
1741-3141	17 41 54.1	-32 41 30.1	140.6 ± 15	35.6 ± 5
1741-3227	17 41 38.7	-32 27 29.9	263.9 ± 15	38.3 ± 5
1741-3245	17 41 38.6	-32 45 30.0	92.4 ± 15	29.6 ± 5
1741-3314	17 41 31.3	-33 14 00.0	119.1 ± 15	32.1 ± 5
1742-3313	17 42 49.0	-33 13 44.8	219.6 ± 20	57.1 ± 5
1742-3222	17 42 27.2	-32 22 14.9	631.6 ± 33	191.4 ± 5
1742-3333	17 42 32.4	-33 33 30.4	71.8 ± 15	19.8 ± 2
1743-3309	17 43 04.5	-33 09 59.0	606.5 ± 20	173.7 ± 5
1743-3313	17 43 05.8	-33 13 14.3	77.6 ± 20	33.1 ± 5
1744-3251	17 44 22.4	-32 51 19.3	106.8 ± 15	37.3 ± 2
1746-3259	17 46 18.8	-32 59 44.0	487.3 ± 15	120.5 ± 2
1740-3251	17 40 26.9	-32 51 02.7	103.4 ± 15	48.6 ± 2
1748-3241	17 48 31.1	-32 41 00.8	1211.0 ± 15	412.5 ± 2
1743-3238	17 43 06.6	-32 38 06.4	91.1 ± 15	10.2 ± 2
1742-3241	17 42 26.9	-32 41 00.7	293.6 ± 15	243.0 ± 2

Table 6.5: List of point sources and their 327- and 1400-MHz flux densities in the field of G358.3+3.8

Name	RA_{J2000} ($h\ m\ s$)	Dec_{J2000} ($^\circ\ '\ ''$)	S_{327} (mJy)	S_{1400} (mJy)
1728-28	17 28 28.9	-28 46 03.5	1605.4 ± 25	567.2 ± 3
1727-28	17 27 01.9	-28 15 55.5	87.4 ± 25	104.5 ± 3
1725-28	17 25 20.3	-28 05 19.8	386.4 ± 25	130.2 ± 3
1724-28	17 24 17.7	-28 06 05.6	812.1 ± 25	167.2 ± 3
1724-29	17 24 19.5	-29 01 05.8	244.9 ± 25	125.4 ± 3
1727-28	17 27 39.8	-28 59 06.2	299.5 ± 25	117.1 ± 3
1727-28	17 27 42.3	-28 40 42.1	154.8 ± 25	34.7 ± 3
1727-28	17 27 22.9	-28 19 42.9	153.9 ± 25	98.5 ± 3
1727-28	17 27 34.6	-28 15 18.4	114.2 ± 25	53.7 ± 3

6.3 Extended sources

6.3.1 G003.6-0.11

This source, seen just west of G003.7−0.2 in the 1428 MHz image by Gaensler (1999), is also detected as a resolved source at 327 MHz. The GMRT 327-MHz image and the VLA 1428-MHz images of this sources are shown in Fig. 6.1. The resolution in the 327- and 1428-MHz images is $\approx 20 \times 11$ arcsec^2 and 15×9 arcsec^2 respectively. This source was also observed by Yusef-Zadeh (private communications) using the VLA in the D-array configuration at 4.9 GHz. We therefore mapped this source at 4.9 GHz using the data acquired from the VLA achieves (Fig. 6.2). The size of this source is $\sim 1'$ with the centre located at $\mathrm{RA}_{J2000} = 17^h54^m32^s$, $\mathrm{Dec}_{J2000} = -25^\circ51'30''$. There is significant emission in the IRAS 60μm image peaking at $\mathrm{RA}_{J2000} = 17^h54^m32^s$, $\mathrm{Dec}_{J2000} = -25^\circ50'33''$ (Fig. 6.2).

Radio Recombination Lines (RRLs) have been detected towards $\mathrm{RA}_{J2000} = 17^h54^m30^s$, $\mathrm{Dec}_{J2000} = -25^\circ51'23''$ near 5 GHz (H109α and H110α lines) by Caswell & Haynes (1987) using the Parkes 64-m single dish with a HPBW of $\approx 4'$ and by Lockman (1989) at 3 cm with a HPBW of $\approx 3'$. The RRL parameters reported by Caswell & Haynes (1987) are: $T_l/T_c = 0.05/0.7$, $\theta = 2'$, $\Delta V = 28$ km sec^{-1}, $V = 3$ km sec^{-1}, $T_e = 5600$ K, $D = 1.5$ or 15.5 kpc (assuming the standard IAU parameters (Kerr & Lynden-Bell 1986) for solar orbital velocity $\theta_\circ = 220$ km sec^{-1} and distance to the Galactic Centre $R_G = 8.5$ kpc).

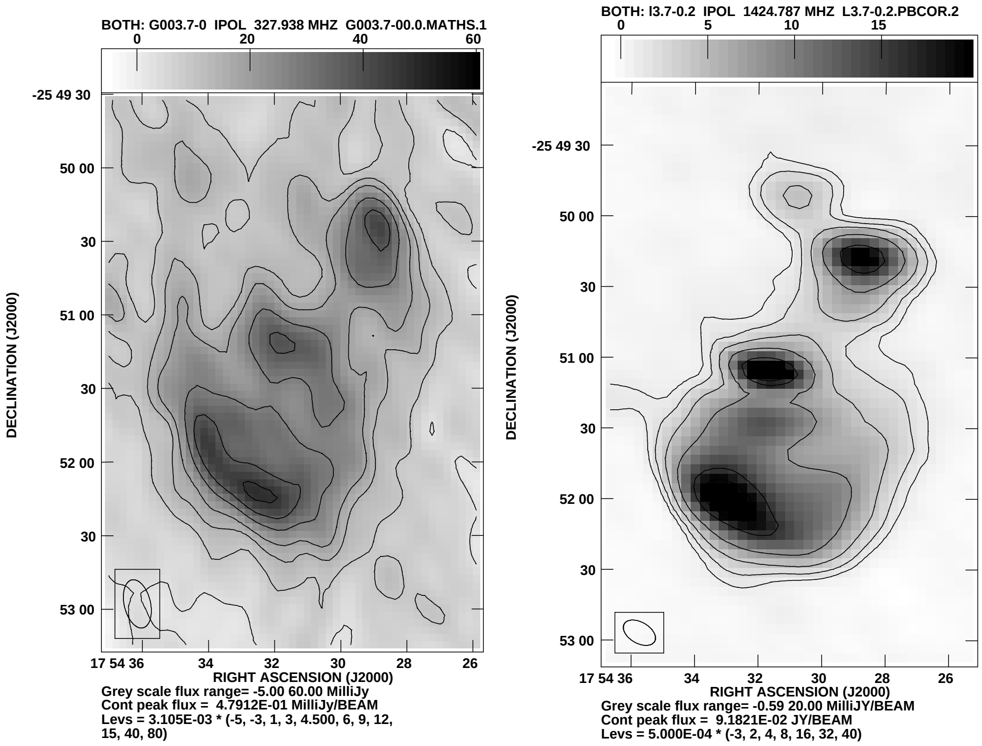

Figure 6.1: The left panel shows the GMRT 327-MHz image of G003.6−0.1. The resolution in this image is $\sim\ 15\times 20\ \mathrm{arcsec}^2$ and the RMS noise of $\sim\ 5$ mJy. The VLA image at 1428 MHz (Gaensler 1999) is shown in the right panel. Resolution in this image is about $15\times 9\ \mathrm{arcmin}^2$. The shell type structure of this object is clearly seen in this image. The general morphology is same as that seen in the 327-MHz GMRT image and the source in the north-west is also resolved as a separate compact source.

However, since the Galactic longitude is small, the measured radial velocity could entirely come from non-circular motion which makes the distance estimates unreliable and must be treated as a nominal distance. No optical counterpart is detected implying that a distance of 15.5 kpc is more likely. The surveys by Downes et al. (1980) and Wink et al. (1983) for H76α and H110α transitions respectively do not detect any RRL towards G003.7−0.1 due to the sensitivity limits of the surveys ($S_{4.9GHz} > 1$ Jy and $S_{14.7GHz} > 2$ Jy respectively). This source is listed as a HII region in the continuum survey done by Wink et al. (1982) at 14.8 and 4.9 GHz (HPBW=$2'.6$) and is also listed in the list of compact sources from the 11 cm Galactic plane survey by Fürst et al. (1990). The PMN source `PMN J1754-2551` at $\mathrm{RA}_{J2000} = 17^h54^m31^s$, $\mathrm{Dec}_{J2000} = -25^\circ51'02''$ covers all the components of

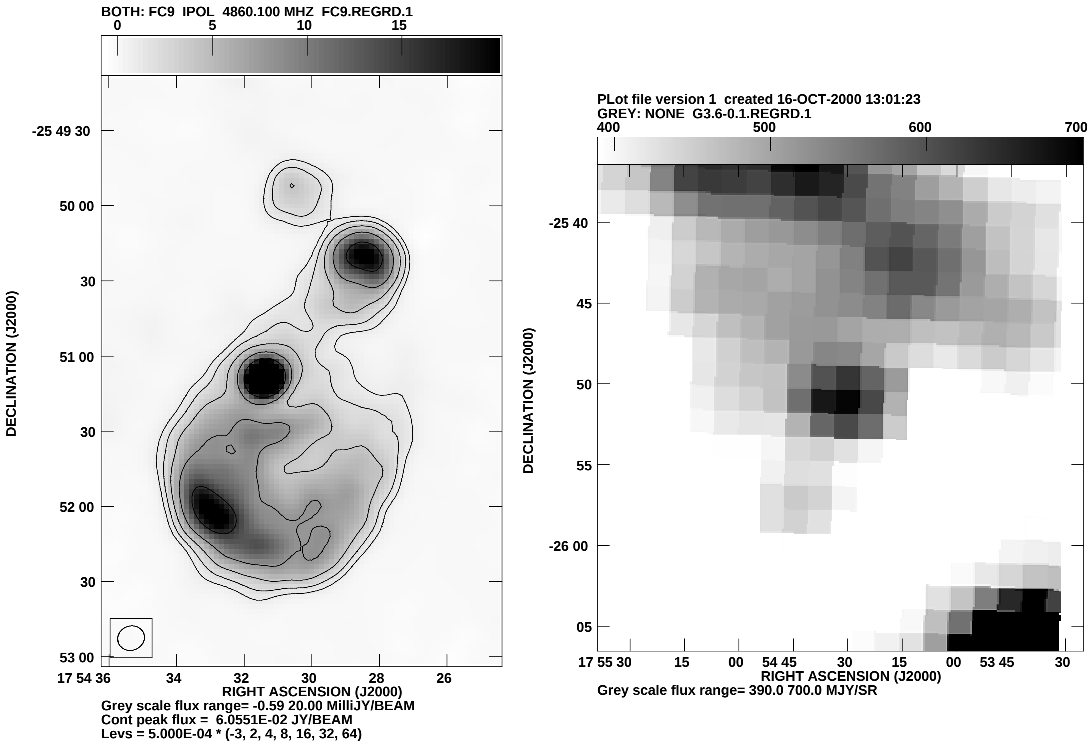

Figure 6.2: The VLA 4.8-GHz image of G003.6−0.1 using the data acquired by Yusef-Zadeh in Feb. 1987 is shown in the left panel. The resolution in this image is $\sim 11 \times 10\mathrm{arcmin}^2$, P.A.=$-70°$. The general morphology of a compact core at the south-eastern edge of the lower surface brightness shell is clearly visible. The right panel shows the IRAS 60 μm image of this region. The peak in this image occurs at $\mathrm{RA}_{J2000} = 17^h54^m32^s$, $\mathrm{Dec}_{J2000} = -25°50'33''$. With the coarse resolution of IRAS, this peak covers the entire radio source.

this source (Griffith et al. 1994).

A circular shell of emssion with a peak of emssion along the southern edge of the shell along with two compact sources in the north is visibile in the 327-, 1428- and 4850-MHz images. For further discussion of the nature of this source, we label the peak of emission in the south-eastern part of the shell as `A`, the shell itself as `B`, the compact source on the northern rim of the shell as `C` and the moderately resolved northern most source as `D`. There is an indication of a connecting bridge of emission between `C` and `D` in all the three images. The disctinct semi circular gap around `C`, followed by a concentric arc seen in both the 5 and 1.4 GHz images is suggestive of an interaction between `A` and `B/C`. HI

Table 6.6: Peak flux densities for the components `A, C` and `D` for G003.6−0.1 at 0.327, 1.4 and 4.8 GHz.

Component	S_{327MHz} (mJy)	$S_{1.4GHz}$ (mJy)	$S_{4.8GHz}$ (mJy)
A	48.2	32.5	33.5
C	38.6	24.8	46.1
D	42.5	22.4	26.2

absorption spectra was measured using the GMRT towards `A, C` and `D` (Fig. 6.3). The HI absorption spectra for `A` and `C` is very similar, implying that they are at a similar kinematic distance. The extra -27 km sec^{-1} feature in the spectra of `D` implies that this component is farther away compared to `A` and `C`. Kinematic distance of `D` corresponds to > 20 kpc and could also be extragalactic. The V_{LSR} of 3 km sec^{-1} for the RRL and the $+30$ km sec^{-1} feature seen in the spectra of all the three components implies that the line of sight absorber at a velocity of $+30$ km sec^{-1} is not associated with the RRL emitter. This absorber corresponds to a kinematic distance between 6 and 12 kpc. Assuming that the RRL is associated with extended nebula and the component `A`, a distance of 15.5 kpc is then consistent with the RRL and HI absorption velocities. The absence of the -27 km sec^{-1} feature in the spectra of `A` and `C` places these components in front of the component `D` and consequently the component `D` at > 20 kpc.

However, HI absorption at negative velocities are observed in the first quadrant of the inner Galaxy, possibly from clouds in the Galactic Centre region. If the observed RRL is `not` associated with the nebula or any of the components, and the -27 km sec^{-1} feature is due to line of sight clouds with anomalous chaotic motions (Shaver et al. 1982; Belfort & Crovisier 1984), the HI absorption profiles are consistent with components `A` and `C` at a distance between R_G and 6 kpc, while `D` at a distance $> R_G$. This ambiguity can be resolved with a high resolution RRL observation towards this direction to identify the RRL emitter.

The peak flux densities of the components `A,C` and `D` were measured from the 0.327, 1.4 and 4.8 GHz maps after convolving them to same resolution. The measured peak flux densities are listed in Table 6.3.1 and plotted in Fig. 6.4. Emission from the nebula itself is indicative of non-thermal emission. At 327 MHz, `C` does not appear to be distinct from the shell and the flux density at this frequency may be contaminated by that due to the

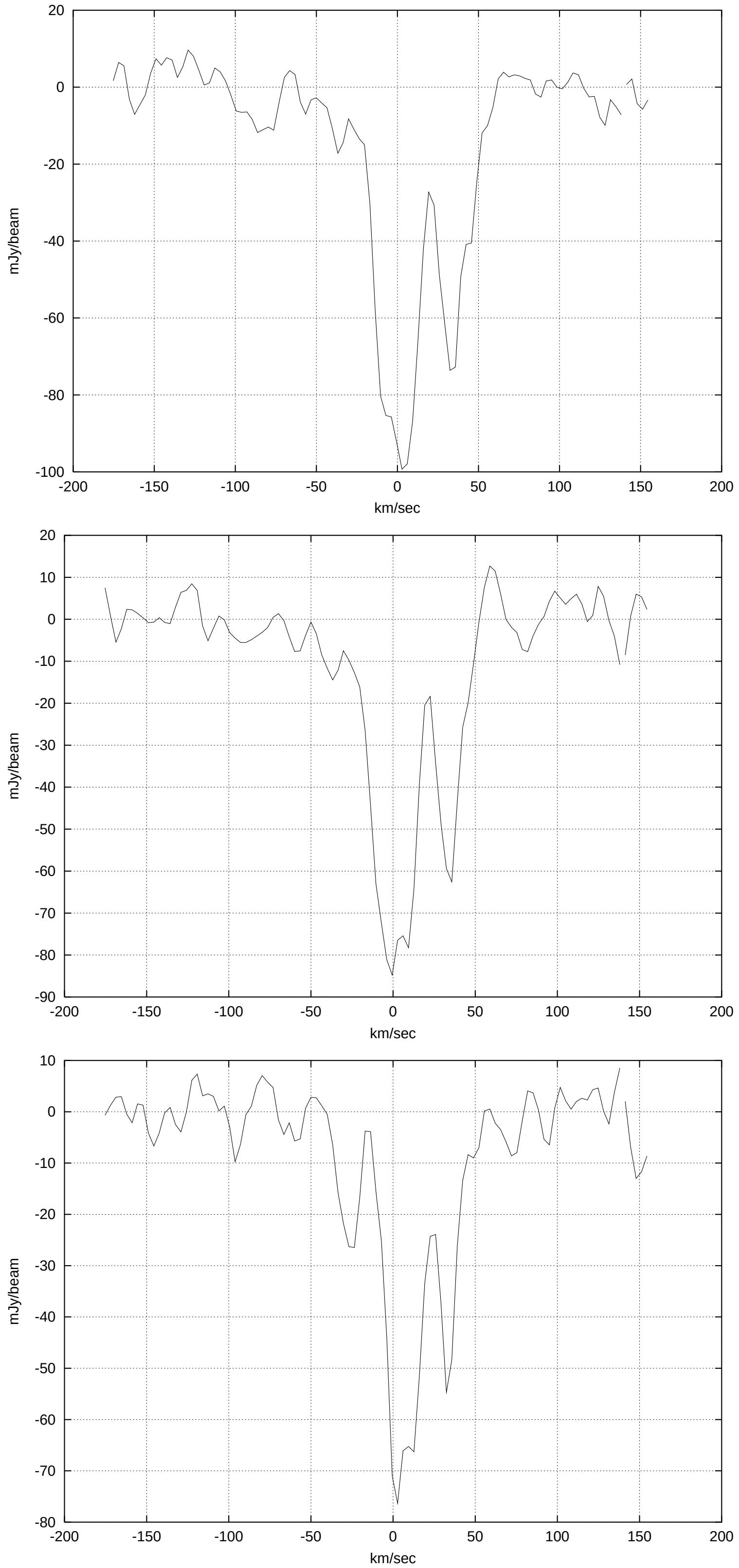

Figure 6.3: HI absorption profiles against the components `A`, `C` and `D` of G003.6−0.1 respectively, measured using the GMRT.

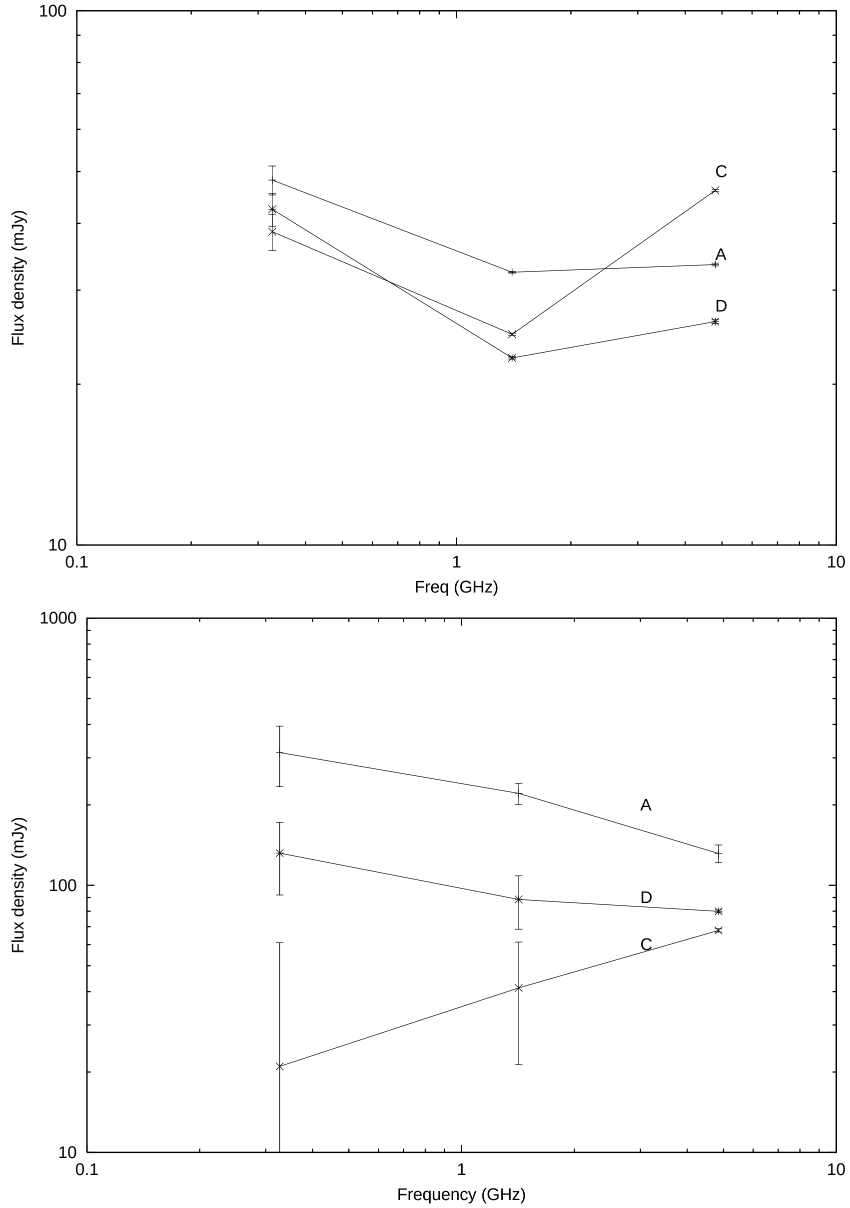

Figure 6.4: Continuum spectra of the components `A, C` and `D` of G003.6−0.1. Top panel shows the peak flux density spectra. The spectral index of component `C` between 1.4 and 4.8 GHz is ~ 0.5 while that of components `A` and `D` are 0.0 and 0.1 respectively. Bottom panel shows the integrated flux density spectra for the three components with the average 327-MHz flux density in the vicinity subtracted for the components `D` and `C` which are not distinctly detected as separate sources at 327 MHz.

shell itself. The 327-MHz flux density of `D` too may thus be contaminated. Subtracting the average flux density measured around these components may give an estimate of the 327-MHz flux density of these components. The bottom panel of Fig. 6.4 shows the integrated flux density spectra of the three components, with the average 327-MHz flux density in the vicinity of components `C` and `D` subtracted. `A` and `D` in this plot show non-thermal spectra. The spectrum of `C` is consistent with spectral index of ~ 0.5 between 327 MHz and 4.8 GHz. The spectral indices thus determined, however, must be treated as only tentative. Observations at other frequencies between 327 and 1400 MHz (e.g. 610 MHz) will help in clarifying the spectra and the nature of these components. The peak flux spectral index between 4.8 and 1.4 GHz ($\alpha_{1.4}^{4.8}$) for the components `A, C` and `D` was measured to be 0.0, 0.5 and 0.1 respectively while the spectral index between 1.4 and 0.327 GHz ($\alpha_{0.327}^{1.4}$) was measured to be -0.3, -0.3 and -0.5 respectively.

Could it be that the 327-MHz flux density is over-estimated and the true value is less than the value at 1428-MHz, as expected from a source of thermal emission? For this to happen, the 327-MHz flux density must be over estimated by a factor of about $\sim 2-3$, which is very unlikely. Another way the flux density can be over estimated is due to a slowly varying background emission. The average flux density in an approximately $1'$ box around this source is ≈ 0.15 Jy, comparable to the error bar of 0.1 Jy for the measured flux density. Hence, this also cannot account for an over estimated flux density. To further eliminate the possibility of a systematic flux density calibration error, we compared the flux densities of the VLA calibrator in the field located at $Dec_{J2000} = 17^h 51^m 52^s$, $RA_{J2000} = -27°24'01.33''$ and the SNR G003.7−0.2. Unfortunately, this VLA calibrator is not a good P-band calibrator and hence the VLA 327-MHz flux density is not known. However, it is listed in the Texas catalogue, and at 365 MHz, its flux density is 1.41 ± 0.09 Jy corresponding to 1.14 ± 0.09 Jy at 327 MHz (spectral index of 1.8 ± 0.7). The measured flux density from the GMRT primary beam corrected image is 1.3 ± 0.2 Jy. The flux density measured for G003.7−0.2 (see section 5.3.1) was also found to be in good agreement with the extrapolated value at 327 MHz.

We now suggest a model for the compact source `C`. The class of symbiotic stars is defined by the basic characteristic of an optical spectrum containing both high excitation emission lines and absorption features of a cool, late-type star (Seaquist & Taylor 1990). While most of these stars emit radiation at IR wave bands, few of these stars are also detected at radio frequencies. High frequency (GHz range) spectral index is invariably positive, ranging from 0 to 1.2 and the emission mechanism is thermal bremsstrahlung. This range of spectral indices can be explained by a simple binary model, where, the wind in the form of uniform mass loss from a cool star is ionized by a hotter companion star (Taylor & Seaquist 1984). This model predicts a lower limit of 0.6 and an upper limit of 1.3 for the spectral index, depending upon the viewing angle of the binary system, the mass loss rate from the cooler star and the ionizing photon flux from the hotter star. Some fraction of the emission, however, might be optically thin and an observed optically thick spectral index lower than 0.6 may be consistent with the binary model. The radio spectra of most of these stars, above a few GHz, turn over to a relatively flat spectral index of ~ 0.1. A radio survey of such stars in the Galaxy done by Seaquist et al. (1984) found a mean spectral index of $+0.6$ and a cut off at 1.2, in excellent agreement with the binary model.

The high frequency spectral index ($\alpha_{1.4}^{4.8}$) of component C is therefore consistent with it being such a radio loud symbiotic star. The binary-model for such objects relates the turn-over frequency and the optically thick spectral index to the physical properties, namely the mass-loss rate and the hydrogen ionizing photons flux. The present high frequency data on this source probably samples only the optically thick part of the spectrum. Continuum observations a few higher frequencies will be required to determine the true nature of this source.

About 20% of the UC H II regions mapped in the incomplete survey of Wood & Churchwell (1989b) and Kurtz et al. (1994) where of the cometary morphology. A typical example of this morphology is G034.2−0.2. van Buren et al. (1990) proposed a model of a bow shock created by a wind-blowing massive star moving supersonically through a molecular cloud. The required velocities of less than ~ 10 km sec^{-1} are comparable to the observed velocity dispersion of stars in OB associations. The gross structure seen in the radio continuum and the velocity structure in the hydrogen recombination and molecular lines is well explained by this model. Their model also make specific predictions about the OH maser spots in the leading edge of the shock as well as detectable proper motion of maser sources over a time scale of few years for the nearby UC H II region.

The higher frequency spectra of component A is flatter, typical of HII regions. The morphology of the nebula associated with the component A, as seen in the images at 1.4 and 4.8 GHz is suggestive of a cometary UC H II region. A typical UC H II region has a size of < 0.1 pc, $n_e > 10^4 \mathrm{cm}^{-3}$, and EM$> 10^7 \mathrm{pc\,cm}^{-6}$. The linear sizes of the nebula corresponding to the distances of 18.5 and 7 kpc is ~ 1.5 and ~ 5 pc respectively. Clearly, the size of the nebula in this field is much greater than the size of typical UC H II region. However, the extended emission seen towards this source could then have the same origin as the extended emission seen associated with UC H II regions in recent observations at 1.4

and 5 GHz (Kurtz et al. 1999; Kim & Koo 2001). EM for this sources, assuming $T_e = 5600$K as derived from the RRL observations, is also smaller than the typical value for UC H II region. However, the T_e estimates from the existing low resolution RRL observations may be underestimated.

The morphology in the 327-MHz image of this sources is markedly different from that at 1.4 and 4.8 GHz. The brightness contrast between the component `C` and the extended emission associated with the nebula is negligible. The structure of the nebula itself is replaced by two arcs of emission of comparable brightness. The flux density of all the three components at 327 MHz are higher than the values at higher frequencies, which is inconsistent with a purely thermal emission. The 327-MHz data is therefore suggestive of a foreground source of non-thermal emission. The spectra of `A` (Fig. 6.4) between 327 MHz and 4.8 GHz is also non-thermal with a spectral index of ~ -0.4. The spectral index, which is typical of shell-type SNRs, and the morphology seen in the 327-MHz image are consistent with the extended emission being a new SNR. High resolution observations at 233 and 610 MHz with the GMRT, along with higher resolution imaging with the VLA at higher frequencies will help in resolving the nature of the shell. A conclusive evidence of non-thermal emission could come from the detection of polarized radio emission.

6.3.2 Linear structure in the field of G356.3$-$1.5

The linear structure seen $\sim 30'$ north-east of the barrel shaped SNR G356.3$-$1.5 in the low resolution image is also clearly visible in the the high resolution image. The sub-image of this structure is shown in Fig. 6.5. The compact unresolved sources (at the ends of the linear structures) are also present in the NVSS image of this region. However, the linear structure is not detected in the NVSS image at 1420 MHz, probably due to the sensitivity and dynamic range limits (due to snapshot uv-coverage) of the NVSS in this region. Its detection in the GMRT 327-MHz image at the level of $5-7$ mJy/beam, compared to its non detection in the NVSS image, is indicative of non-thermal emission. To eliminate the possibility of this feature being an artifact of data processing or due to the presence of bad data, this data was mapped at low and high resolution. Maps were also made using a single frequency channels as well as using a number of RFI free frequency channels. The low resolution map was made using only the GMRT *Central Square* antennas at a resolution of $3-4$ arcmin which does not require 3D imaging. The high resolution map used all the available arm antennas and required 3D imaging. Multiple frequency channels were used in two ways. Five adjacent frequency channels were averaged and four of these av-

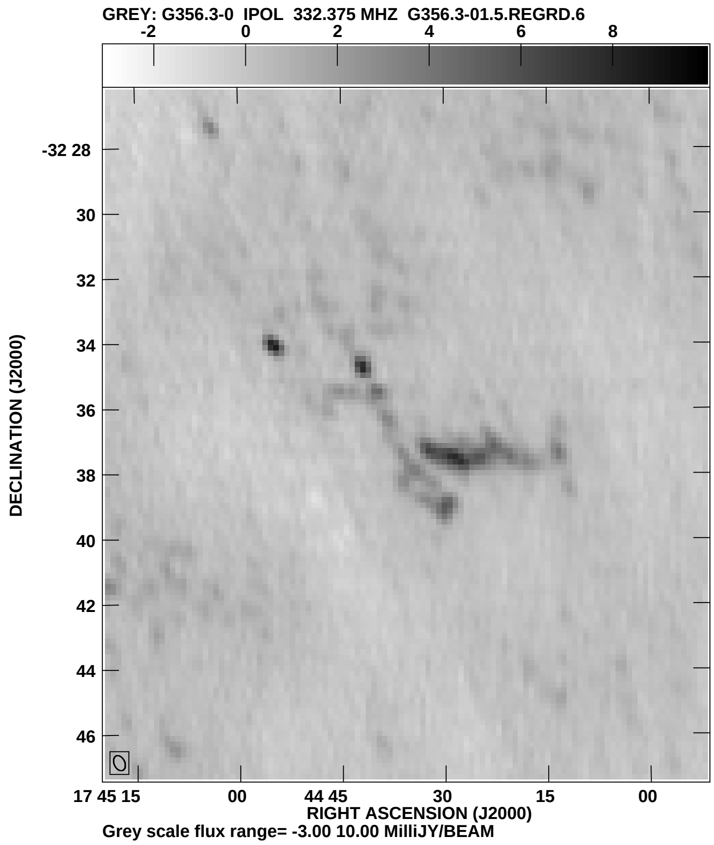

Figure 6.5: Sub-image of the linear structure seen in the full primary beam image of the region containing G356.3−1.5. This structure is seen clearly in the low resolution image as well (Fig. 4.8) and appears to be a real feature and not an artifact.

eraged channels (corresponding to twenty frequency channels at the original frequency resolution) were used for gridding the visibilities. In the second method, all twenty frequency channels were used directly for gridding. This linear structure was seen in all these images.

Marginally extended linear features similar to this structure (see also the lower resolution image in Fig. 4.8) have been detected earlier in the 843 MHz survey of the inner Galaxy (Gray 1996). One such feature, namely G357.1−0.2, was later imaged at higher resolution using the VLA at 5 GHz revealing a bizarre source with 'tubes' of highly confined emission in an even more bizarre morphology. The nature of this source, which is fairly close to the Galactic plane, is not known. The extended structure seen in this GMRT image is also suggestive of a similar source. Higher resolution continuum imaging, polarimetry and HI absorption observation towards this source will be required to get some handle on its nature.

6.4 Extended emission around Ultra Compact HII regions

6.4.1 G004.417+0.126

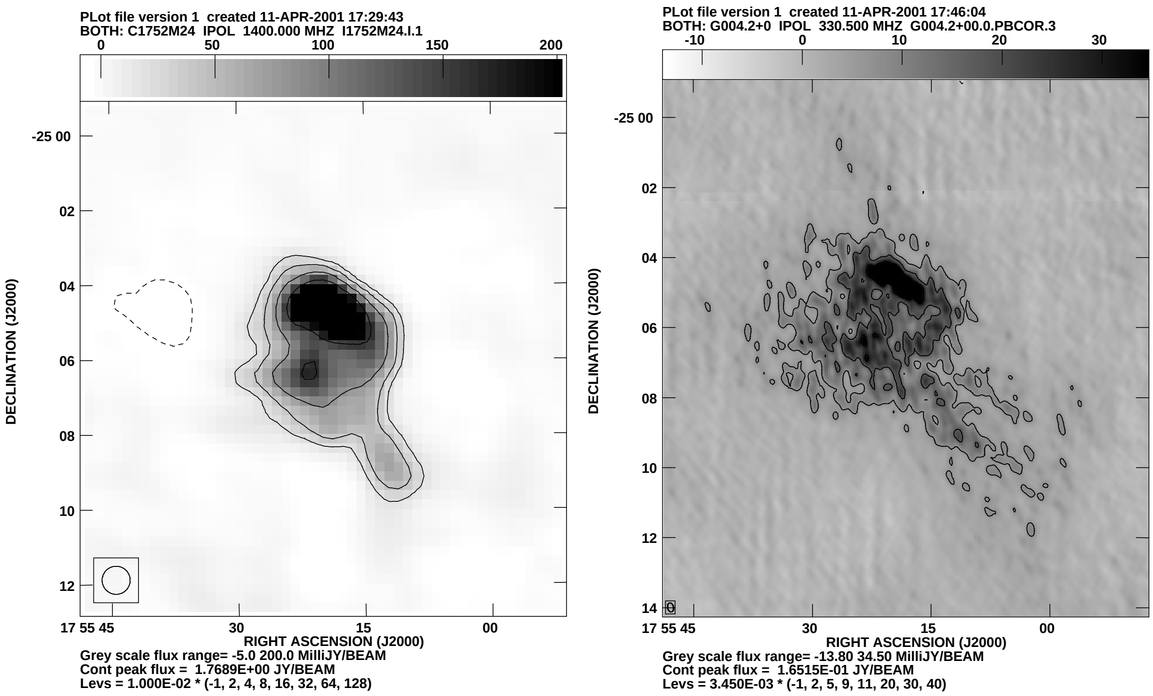

Figure 6.6: The left panel shows the NVSS image of the Ultra Compact H II region G004.4+0.1 at 1420 MHz. The RMS noise in this image is ~ 0.5 mJy and the resolution of $\sim 45 \times 45\ \mathrm{arcsec}^2$. The right panel shows the 327-MHz image. The resolution in this image is $\sim 15 \times 11\ \mathrm{arcsec}^2$ and the RMS noise of ~ 3.5 mJy.

This source, visible in the 327-MHz GMRT image as well as in the 1420-MHz NVSS image (Fig. 6.6), coincides with a an UC H II region G004.417+0.126 (Becker et al. 1994) (classified on the basis of its high frequency flux densities and IR colour selection criteria (Wood & Churchwell 1989a,b)). Images of this source at 327 MHz from the GMRT and 1420 MHz from the NVSS presented here are the first resolved images of this source. The extended emission around a compact core seen these images is similar to that detected for other UC H II regions using the VLA in D-array configuration (Kurtz et al. 1999; Kim & Koo 2001).

The peak flux densities measured at 327 and 1420 MHz, from images smoothed to the same resolution, are 0.49 and 0.51 Jy respectively. The spectral index between 327 and 1420 MHz corresponding to these values is close to zero and is consistent with this being a flat spectrum thermal source. The integrated flux densities from the 5 and 1.4 GHz Galactic plane surveys (Becker et al. 1994) however corresponds to a negative spectral index between 5 and 1.4 GHz (the 1.4 GHz flux density from their measurement is in fact underestimated due to missing flux for sources larger than 120 arcmin; inclusion of the missing flux will make the spectral index more negative). Cuts taken across the spectral index map made using the images at 327 and 1400 MHz are shown in Fig.6.7. The spectral index of the compact core is reasonably flat between 1.4 GHz and 327 MHz. Here also, away from the core, the spectral index is negative, indicative of non-thermal component of emission (neither of these images suffer from missing flux). The average spectral index measured from the resolved images at these frequencies also show a gradient from nearly zero for the core to ~ -0.3 for the nebula.

In the far infrared colour-colour plot of $\log(S_{25\mu m}/S_{12\mu m})$ vs. $\log(S_{60\mu m}/S_{12\mu m})$ (Wood & Churchwell 1989a), UC H II regions are concentrated in the upper left quadrant of the plot (around $\log(S_{25\mu m}/S_{12\mu m}) \approx 1.0$ and $\log(S_{60\mu m}/S_{12\mu m}) \approx 2.0$). The IRAS flux densities for this source are 16.07, 132.7, 1010 and 2748 Jy at 12, 25, 60 and 100μ m respectively (Becker et al. 1994). On the IR colour-colour plot, this source lies at $\log(S_{25\mu m}/S_{12\mu m}) \approx 0.9$ and $\log(S_{60\mu m}/S_{12\mu m}) \approx 1.8$, which indicates that this is an UC H II region. H85α RRL transition at $V_{LSR} = 4.1$ km sec^{-1} has also been detected towards this direction (Lockman 1989). This puts a lower limit on the linear size of a few pc corresponding to the observed angular size of ~ 4 arcmin and a distance corresponding to systemic velocity of the RRL towards this source. Again, this is large compared to the typical size for the UC H II regions (< 0.1 pc). EM of $\sim 11 \times 10^7$ pc cm^{-6} for this source, using the peak flux density at 5 GHz and assuming $T_e = 10^4$ filling the resolution element, is consistent with this source being a UC H II region (Wood & Churchwell 1989b).

Recent detection of associated extended emission around many of the so called UC H II regions (Koo et al. 1996; Kurtz et al. 1999; Kim & Koo 2001) is on a similar scale as the extended emission seen for this source. The extended emission seen in the 327 and 1400-MHz images is therefore not surprising; the advantage of high resolution provided by the GMRT simultaneously with sensitivity to large angular scales is apparent. However, it

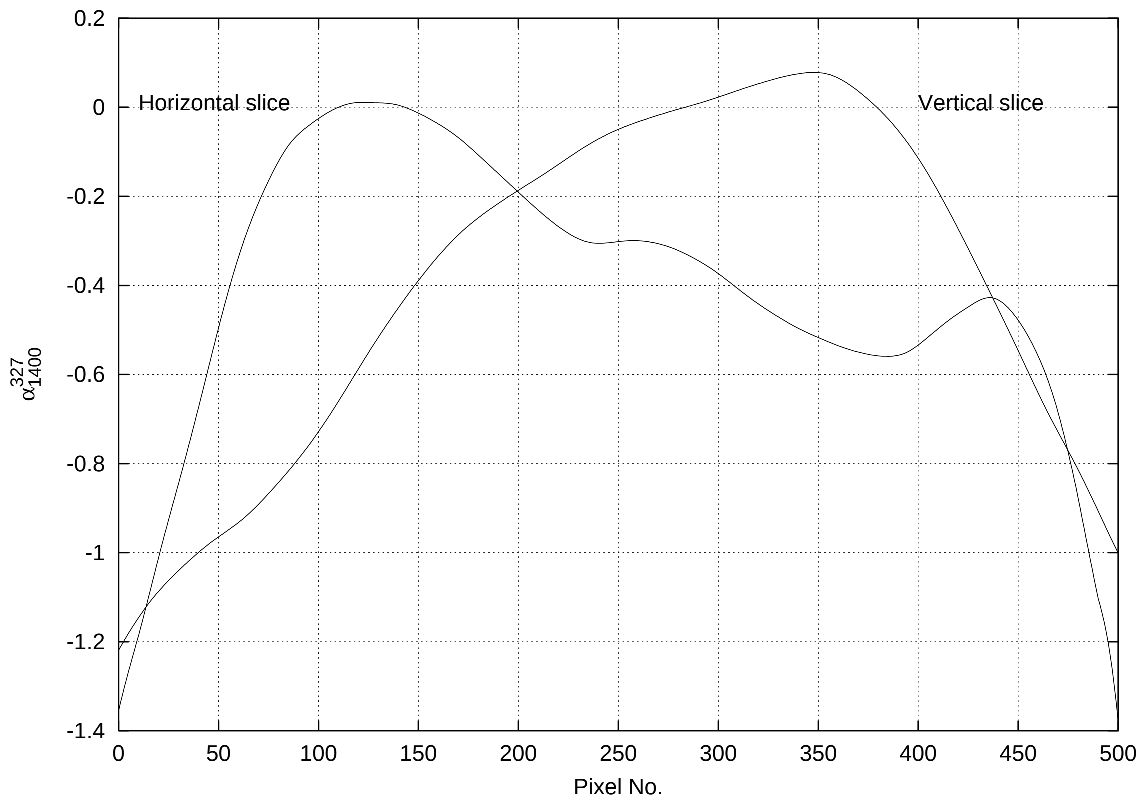

Figure 6.7: Plot of vertical and horizontal slices of the spectral index map between 327 and 1400 MHz taken across the compact core of G004.417+0.126. The compact core exhibits flat spectrum while the extended emission around the core has a steeper spectrum.

is unclear what ramifications this extended emission might have on the models that attempt to explain the morphology of UC H II regions (Kurtz 2000). Scaled versions of current models are unlikely to explain the emission at arcmin scales. Similarly, the spectral index variation across the source (from the compact core to the extended component) is harder to explain.

6.4.2 G003.349−0.076

Two UC H II regions, namely G003.349−0.076 and G003.351−0.077 (Becker et al. 1994) lie at the edge of the field containing the barrel shaped SNR G003.6−0.2. The location of these objects coincides with the northern most compact peak of emission in the subimage of this region shown in Fig. 6.8. Extended emission in the immediate vicinity of these compact sources on the scale of several arc-seconds to several arc-minutes is also

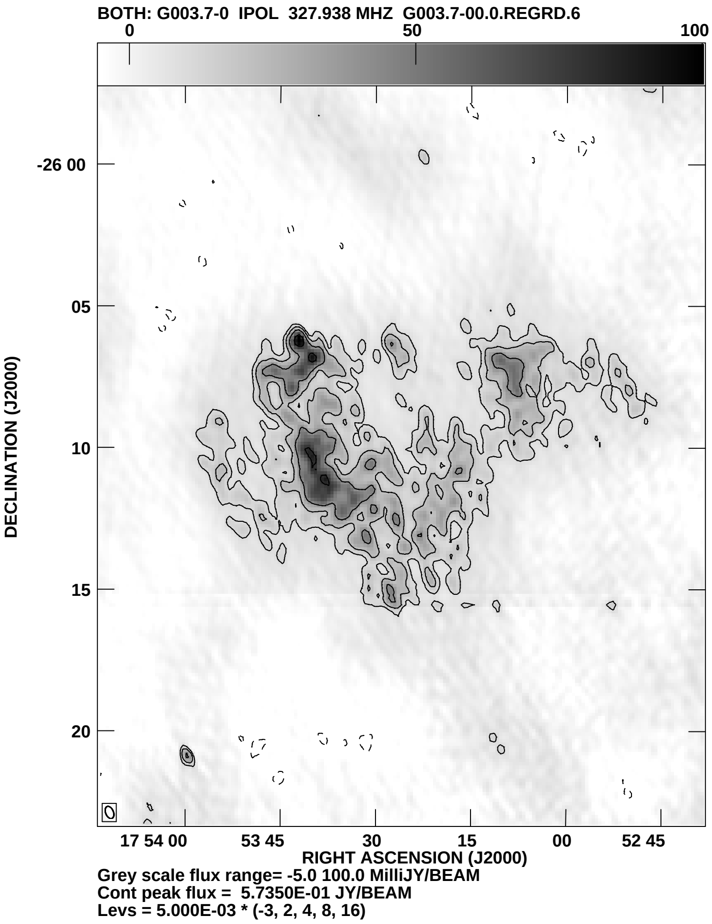

Figure 6.8: Sub-image showing extended emission around two catalogues Ultra Compact H II regions located at $\mathrm{RA}_{J2000} = 17^h53^m41^s$, $\mathrm{Dec}_{J2000} = -26°06'08''$ and $\mathrm{RA}_{J2000} = 17^h53^m41^s$, $\mathrm{Dec}_{J2000} = -26°06'04''$. The resolution in the image is $\sim 20 \times 10$ arcsec^2 and the RMS noise ~ 5 mJy/beam.

clearly visible in this image. The quality of the image for this region is, however, not very good, possibly due to primary beam attenuation as well as due to antenna tracking errors on some of the antennas due to which sources on the edge of the beams suffer from effective differential short time scale gain changes. The precise morphology of this extended emission as well as the flux density of this emission, therefore, cannot be reliably determined from this image. High resolution observations, centred on this region at a few frequencies, using the GMRT will be required to determine the nature of this extended emission.

6.5 Discussion

With the GMRT field of view of $\sim 1^\circ.4$ at 327 MHz, low frequency mapping in the Galactic plane reveal a variety of sources of compact as well extended emission. The GMRT observations of many the objects presented here, are the first high resolution observations at these low frequencies. With the *Central Square* providing reliable measurements up to $\sim 100\lambda$, these measurements are also sensitive to angular scales of up to ~ 30 arcmin. Emission at such large scales with a sub-arcsecond resolution and sensitivity of $5-20$ mJy/beam detects large and small scale structures, not detected in other earlier observations in the Galactic plane. High resolution imaging at other GMRT frequencies of the objects discussed here will provide additional information, not available from any other observation, which will help in determining the nature of these sources. In particular, thermal and non-thermal emission can be separated using the difference in the continuum spectra at these frequencies. Detailed spectral index changes within extended objects, which provides unique information about the emission mechanisms, physical parameters of the objects (e.g. H II and UC H II regions, SNRs) as well as information about the parameters of the intervening ISM, can be studied using such observations.

From the available data for G003.6−0.1, components `A` and the associate extended emission indicates that the emission is non-thermal. At higher frequencies, `C` and `D` are seen as distinct compact sources. The spectra of `C` is consistent with it being a radio loud symbiotic star. HI absorption spectra towards these three components show that `D` is farther away and probably an extragalactic background source. `A` and `C` are at similar kinematic distance and the ridge of emission seen clearly in the 5 GHz image, and marginally in the 1420 MHz image is indicative of an interaction between `C` and the extended emission. Continuum observations at 8 and possibly at 15 GHz with the VLA are needed to conclusively determine the nature of these objects. Spectral index of the emission from the shell can be measured using continuum images from the GMRT at 233 and 610 MHz. High resolution RRL observations towards G003.6−0.1 are also required to determine the source of RRL detected at 5 GHz from this direction.

The linear extended object see in the field of G356.3−1.5 is similar to that detected earlier by Gray (1996). Higher resolution observations, and if possible, measurements of polarization properties of this object are required to further ascertain the nature of this object.

327-MHz images of the UC H II regions, namely G004.4+0.1, G003.349−0.076 and G003.351−0.077, are the first images which resolve the low frequency extended emission from these fields. The morphology of G004+0.1 seen in this image is typical of UC H II regions. However, the liner size of ~ 5 pc is too large compared to the size of < 0.1 pc of typical UC H II regions. Extended emission at 327 MHz in the immediate vicinity of G003.349−0.076 and G003.351−0.077 is also detected.

Extended emission around UC H II regions at angular scales of several arcmins (corresponding to linear sizes in the range of $2 - 20$ pc) have been recently detected at 5 and 1.4 GHz D-array VLA observations (Koo et al. 1996; Kim & Koo 2001). These extended components have been found to be kinematically and certainly morphologically associated with the compact components and it appears that the ionizing source of for the extended and compact components is same.

About 1000 UC H II regions have been identified so far. This gave rise to what is referred to as the "age problem" (de Pree et al. 1995, and reference therein): the number of UC H II regions estimate from the IRAS $60 - 12$ μm and $25 - 12$ μm colours, is about an order of magnitude greater than expected from other indicators of massive star formation rate based on their dynamical age (Wood & Churchwell 1989a,b). From this, it is inferred that the life of the ultra-compact phase of H II regions is $\geq\sim 10^5$ yr, larger by an order of magnitude than their sound crossing time ($\leq\sim 10^4$ yr). Most of these UC H II regions were identified from their small size (≤ 0.1 pc) and high interfered electron density ($n_e \geq 10^4$ cm^{-3}). Recently, VLA D-array imaging of an UC H II region (G005.58−0.24) revealed emission at scales ranging from 0.04 to 40 pc (Koo et al. 1996) which appeared morphologically associated with the UC H II region. It has an ultra-compact core, a compact core, an extended halo and a large diffused plateau. This prompted observations of a randomly selected sample of UC H II regions using the VLA at 3.6 cm in the D-array configuration (Kurtz et al. 1999). These observations revealed extended emission around compact cores in 12 out of 15 sources. More recently, in a survey by Kim & Koo (2001) of 16 UC H II regions using the VLA (DnC array) at 1.4 GHz, extended emission at scales of $2 - 12$ arcmin ($4 - 19$ pc) is detected in *each* one of the fields. It, therefore appears, that the previous classification of UC H II region was essentially based on high resolution observations with the VLA, which suffered from the selection effect due to the insensitivity to large scale emission and therefore revealed only the compact/ultracompact core. It now appears that the UC H II regions may be just the compact cores of larger HII regions. Evidence of this association comes from the tight correlation between the velocities of the UC H II regions, compact components and the extended envelopes (Kim & Koo 2001). The fact that the extended envelopes are detected in such a large fraction of UC H II regions in observations which *are* sensitive to large scale emission further indicates that the extended emission is associated.

The implications of a physical association of this extended emission with compact cores are far reaching. Kim & Koo (2001) estimate that most sources known as UC H II regions are likely to be associated with extended emission. Existence of extended emission at scales $\geq\sim$ few pc, ionized by the same sources, implies that the actual age of the so-called UC H II regions is $\geq\sim 10^4$ yr which could mitigate the "age problem" (de Pree et al. 1995). The IRAS colour criteria may select compact or extended H II regions, as well as UC H II regions - an idea consistent with the results of Codella et al. (1994) who found that more than half of the 445 diffuse H II regions are related to IRAS points sources which satisfy this colour criteria. No variation in the IRAS colours was also found for UC H II regions with evidence of extended emission, implying that the colour criteria is insensitive to the presence of extended emission, and a significant fraction of IRAS colour selected UC H II regions may have associated extended emission.

It therefore appears that the sequence of observations based, first on the selection of sources based on IRAS colours and then high resolution radio observations, which led to the "identification" and classification of UC H II regions is fraught with severe selection and observational biases. If most of the so-called UC H II regions have extended emission associated with them, these UC H II regions may be just compact cores, possibly composed of several compact components, of large HII regions. Observations of a larger sample of such sources with the GMRT, which provides *simultaneous* high resolution and sensitivity to large scale emission, will greatly help in settling the issue of the existence of associated large scale emission. None of the models put forth to explain the longevity of UC H II regions predicted the presence of extended emission around them. Kim & Koo (2001) have proposed a model, which is a combination of champagne flow model with the hierarchical structure of massive star-forming regions (Tenorio-Tagle 1982, and references therein). A massive star, which forms off-centre within a hot core, which in turn is embedded in a lower density molecular clump, can produce the compact component seen associated with the UC H II regions due to the hot core. The morphology of this compact component can be explained by the champagne flow, which would develop when the ionizing front breaks out of the core. The HII region inside the hot core continues of be ultracompact, while it grows to ~ 1 pc outside the core. Another champagne flow would develop when the ionization front crosses the edge of the molecular clump, which forms a more extended emission. The morphology in the radio continuum image, as well as the gradient of H76α line emission lends support to this model. However, if most of the so-called UC H II regions show associated emission, it will be difficult to explaining why so many of the UC H II regions would correspond to a situation where the star, the hot core and the molecular clump are all "carefully" arranged to give the desired observed morphology. High resolution observations, sensitive to large angular scales, of a larger sample (preferably a complete sample) of UC H II will be most desirable to make progress on this front.

The integrated spectral index for G004.417+0.126 between 5 and 1.4 GHz exhibits a negative spectral index (< -0.1). This source is well resolved at 327 and 1.4 GHz and from these images, it appears that the compact core has a flat spectrum while the extended emission has a significantly negative spectral index between these frequencies. The images at 327 MHz and 1.4 GHz for G003.349−0.076 are not reliable for the measurement of the spectral index, but there are indications that the extended emission there too has a negative spectral index. Non of models for UC H II regions predict a non-thermal component. The model proposed by (Kim & Koo 2001) for the extended emission, predicts a thermal spectrum for the extended emission. A larger sample of UC H II regions needs to be mapped at 327 MHz and 1.4 GHz to access if a non-thermal component is characteristic of the extended emission around UC H II or these sources are just odd cases, emission from which needs to be explained separately.